Protist, Vol. 165, 493–511, August 2014
http://www.elsevier.de/protis
Published online date 10 June 2014

Protist

ORIGINAL PAPER

Comparative Ultrastructure and Molecular Phylogeny of *Selenidium melongena* n. sp. and *S. terebellae* Ray 1930 Demonstrate Niche Partitioning in Marine Gregarine Parasites (Apicomplexa)

Kevin C. Wakeman[a,1], Matthew B. Heintzelman[b], and Brian S. Leander[a]

[a]Canadian Institute for Advanced Research, Program in Integrated Microbial Biodiversity, Department of Zoology, University of British Columbia, #3529 - 6270 University Blvd., Vancouver, British Columbia V6T 1Z4, Canada
[b]Program in Cell Biology and Biochemistry, Department of Biology, Bucknell University, 203 Biology Building, Lewisburg, Pennsylvania 17837, USA

Submitted October 8, 2013; Accepted May 30, 2014
Monitoring Editor: Frank Seeber

Gregarine apicomplexans are a diverse group of single-celled parasites that have feeding stages (trophozoites) and gamonts that generally inhabit the extracellular spaces of invertebrate hosts living in marine, freshwater, and terrestrial environments. Inferences about the evolutionary morphology of gregarine apicomplexans are being incrementally refined by molecular phylogenetic data, which suggest that several traits associated with the feeding cells of gregarines arose by convergent evolution. The study reported here supports these inferences by showing how molecular data reveals traits that are phylogenetically misleading within the context of comparative morphology alone. We examined the ultrastructure and molecular phylogenetic positions of two gregarine species isolated from the spaghetti worm *Thelepus japonicus*: *Selenidium terebellae* Ray 1930 and *S. melongena* n. sp. The ultrastructural traits of *S. terebellae* were very similar to other species of *Selenidium* sensu stricto, such as having vermiform trophozoites with an apical complex, few epicytic folds, and a dense array of microtubules underlying the trilayered pellicle. By contrast, *S. melongena* n. sp. lacked a comparably discrete assembly of subpellicular microtubules, instead employing a system of fibrils beneath the cell surface that supported a relatively dense array of helically arranged epicytic folds. Molecular phylogenetic analyses of small subunit rDNA sequences derived from single-cell PCR unexpectedly demonstrated that these two gregarines are close sister species. The ultrastructural differences between these two species were consistent with the fact that *S. terebellae* infects the inner lining of the host intestines, and *S. melongena* n. sp. primarily inhabits the coelom, infecting the outside wall of the host intestine. Altogether, these data demonstrate a compelling case of niche partitioning and associated morphological divergence in marine gregarine apicomplexans.

Key words: Apicomplexa; archigregarine; eugregarine; molecular phylogeny; niche partitioning.

[1]Corresponding author; fax +1-604-822-6089
e-mail wakeman.kevin@gmail.com (K.C. Wakeman).

http://dx.doi.org/10.1016/j.protis.2014.05.007

Introduction

Marine gregarine apicomplexans are single-celled parasites with morphologically diverse feeding stages, called "trophozoites", that infect the extracellular spaces of invertebrates. Traits associated with trophozoite morphology and life history dynamics (e.g., asexual division in the trophozoite stage) form the basis for organizing gregarine species into three main groups: archigregarines, eugregarines, and neogregarines (Adl et al. 2012; Cox 1994; Grassé 1953; Leander 2008; Levine 1971, 1976, 1977a, b; Perkins et al. 2002; Schrével 1971a; Théodoridès 1984);. However, molecular phylogenetic data are beginning to refine inferences about the relationships between different species of gregarines by demonstrating several unexpected patterns of divergence, including examples of convergent evolution and significant levels of intraspecific variation in trophozoites (Leander 2007, 2008; Leander et al. 2003; Rueckert and Leander 2009; Rueckert et al. 2010; Rueckert et al., 2011a, 2013; Wakeman and Leander 2012, 2013a, b). Some species of gregarines, by contrast, have trophozoites with morphological traits that have remained relatively unchanged over long periods of time (Leander 2007, 2008; Leander and Keeling 2003; Rueckert and Leander 2009; Schrével 1971a; Simdyanov and Kuvardina 2007; Théodoridès 1984). The molecular phylogenetic data combined with more comprehensive analysis of ultrastructural traits in different species of gregarines are challenging some of the original concepts for the three traditional groupings of gregarines and bring to light a much richer evolutionary history for these parasites (Grassé 1953; Leander 2008; Levine 1971; Rueckert and Leander 2009; Schrével 1971a; Wakeman and Leander 2012).

Archigregarines are found only in marine environments and are inferred to have maintained a set of morphological and life history characteristics from the most recent common ancestor of all gregarines and perhaps apicomplexans as a whole (Grassé 1953, Kuvardina et al. 2002; Leander 2006, 2007, 2008; Leander and Keeling 2003; Leander et al. 2003; Rueckert and Leander 2009; Schrével 1971a). The typically vermiform trophozoites of archigregarines move by rhythmic bending, supported by dense arrays of microtubules beneath the inner membrane system and feed using an apical complex consisting of a closed conoid (Dyson et al. 1993, 1994; Leander 2007, 2008; Leander and Keeling 2003; Schrével 1968, 1971b; Simdyanov and Kuvardina 2007; Stebbings et al. 1974). Phylogenetic trees inferred from small subunit (SSU) rDNA sequences are consistent with the interpretation that archigregarines form a paraphyletic stem group from which other gregarine lineages evolved (Leander 2007, 2008; Rueckert and Leander 2009; Wakeman and Leander 2012). Therefore, improved knowledge of archigregarine diversity at both molecular and ultrastructural levels is expected to shed considerable light onto the earliest stages of apicomplexan evolution.

To this end, we set out to characterize the ultrastructure of *Selenidium terebellae* Ray, 1930 collected from the intestinal lumen of *Thelepus japonicas*. In the process, we discovered a second species that primarily inhabits the coelom of the same host and had trophozoites with a fundamentally different set of morphological traits compared to *S. terebellae*. We comprehensively characterized both species using differential interference contrast microscopy (DIC), fluorescence microscopy, scanning electron microscopy (SEM), transmission electron microscopy (TEM), and molecular phylogenetic analyses of SSU rDNA sequences derived from single-cell PCR. We also used alpha-tubulin antibodies to visualize (1) the distribution of microtubules within trophozoites and (2) the presence or absence of a conoid within the mucron of trophozoites. These data demonstrated novel ultrastructural traits in marine gregarines and the power of molecular phylogenetic data for inferring patterns of morphological divergence that would otherwise be inaccessible from comparative morphology alone.

Results

Morphology of *Selenidium terebellae*

The vermiform trophozoites inhabited the intestinal lumen of the host and were on average 273 μm (range 175 μm - 430 μm, $n = 86$) long and 12 μm (range = 10 μm - 15 μm, $n = 86$) wide (Fig. 1). Cells were capable of bending and twisting and were light brown from the presence of amylopectin granules. A spherical nucleus was located in the center of the cell and had an average diameter of 10 μm (range = 9 μm - 12 μm, $n = 52$) (Fig. 1; Table 1). The nucleus was also indented in seven locations to fit the contours of seven longitudinal epicytic folds that ran along the surface the trophozoites (Fig. 2). The cytoplasm contained pinocytotic whorled vesicles, amylopectin granules, Golgi bodies, mitochondria with tubular cristae, putative lysosomes, and four-membrane bound organelles that were reminiscent of apicoplasts in other apicomplexans (Fig. 3).

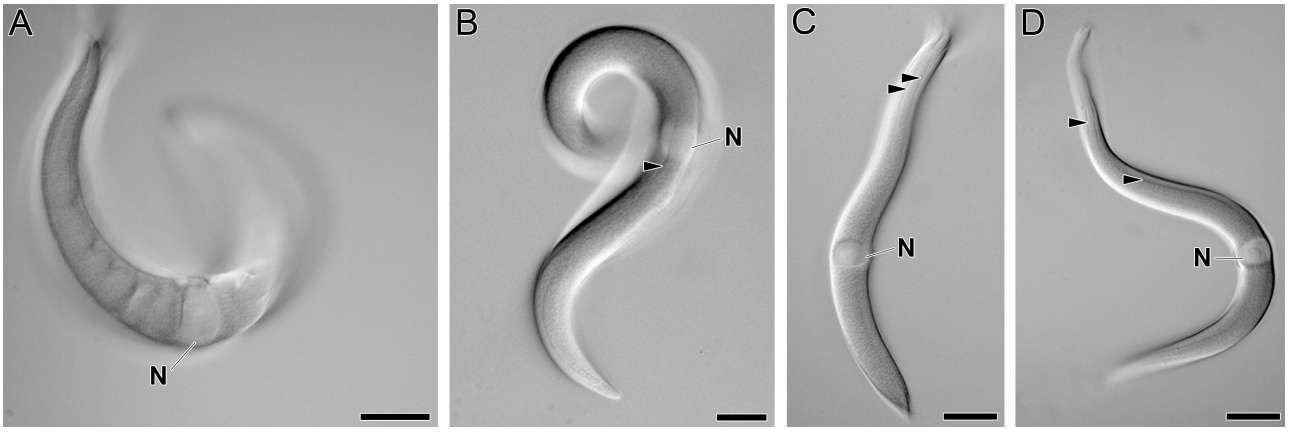

Figure 1. Differential interference contrast (DIC) light micrographs showing the general morphology and bending motility in the trophozoite stage of *Selenidium terebellae*. **A-D.** The nucleus (N) is centrally located in the trophozoite. Epicytic folds (arrowhead) run along the longitudinal axis of the cell. Micrographs are oriented with the mucron towards the top of the figure. Scale bars = 15 μm.

Table 1. Morphological comparison of the trophozoites described in this study, *Selenidium terebellae* and *S. melongena*, and the type species of *Selenidium*, *S. pendula*.

	S. pendula (type)	*Selenocystis foliatum*	*Merogregarina amaroucii*	***S. terebellae***	***S. melongena* n. sp.**
Host	*Nerine cirratulus*	*Scolelepis fuliginosa*	*Amaroucium sp.*	***Thelepus japonicus***	***Thelepus japonicus***
Host tissue	Intestines	Intestines	Intestines	**Intestines**	**Coelom (outside intestine)**
Locality	E. Atlantic	E. Atlantic	SW Pacific	**W. Pacific**	**W. pacific**
Trophozoite shape	Vermiform	Spindle-shaped; vermiform	Oval; "eggplant-shape"	**Spindle-shaped; vermiform**	**Oval; "eggplant-shape"**
Tophozoite size (L x W, μm)	180 x 30-40	30-250 x 10-25	23-31 x 11-15	**175-430 x 10-15**	**30-155 x 10-41**
Nucleus shape	Spherical	Ovoid	Spherical	**Spherical**	**Spherical**
Nucleus size (L x W, μm)	18-33 x 13-32	8-5	9-12	**9-12**	**7-19**
Position of nucleus	Middle	Middle	Middle	**Middle**	**Middle**
Shape of posterior end	Pointed	rounded	Rounded	**Pointed**	**Rounded**
Number of long. epicytic folds	20 to 30	16-24	5-7	**7**	**30**
Transverse surface folds	Unknown	unknown	Unknown	**Yes**	**No**
Shape of mucron	Pointed	bifid/multifid foot-like	Lance-like/Pointed	**Pointed**	**Pointed**
Literature	Levine 1971	Levine 1971; Ray 1930	Levine 1971; Porter 1908	**This study**	**This study**

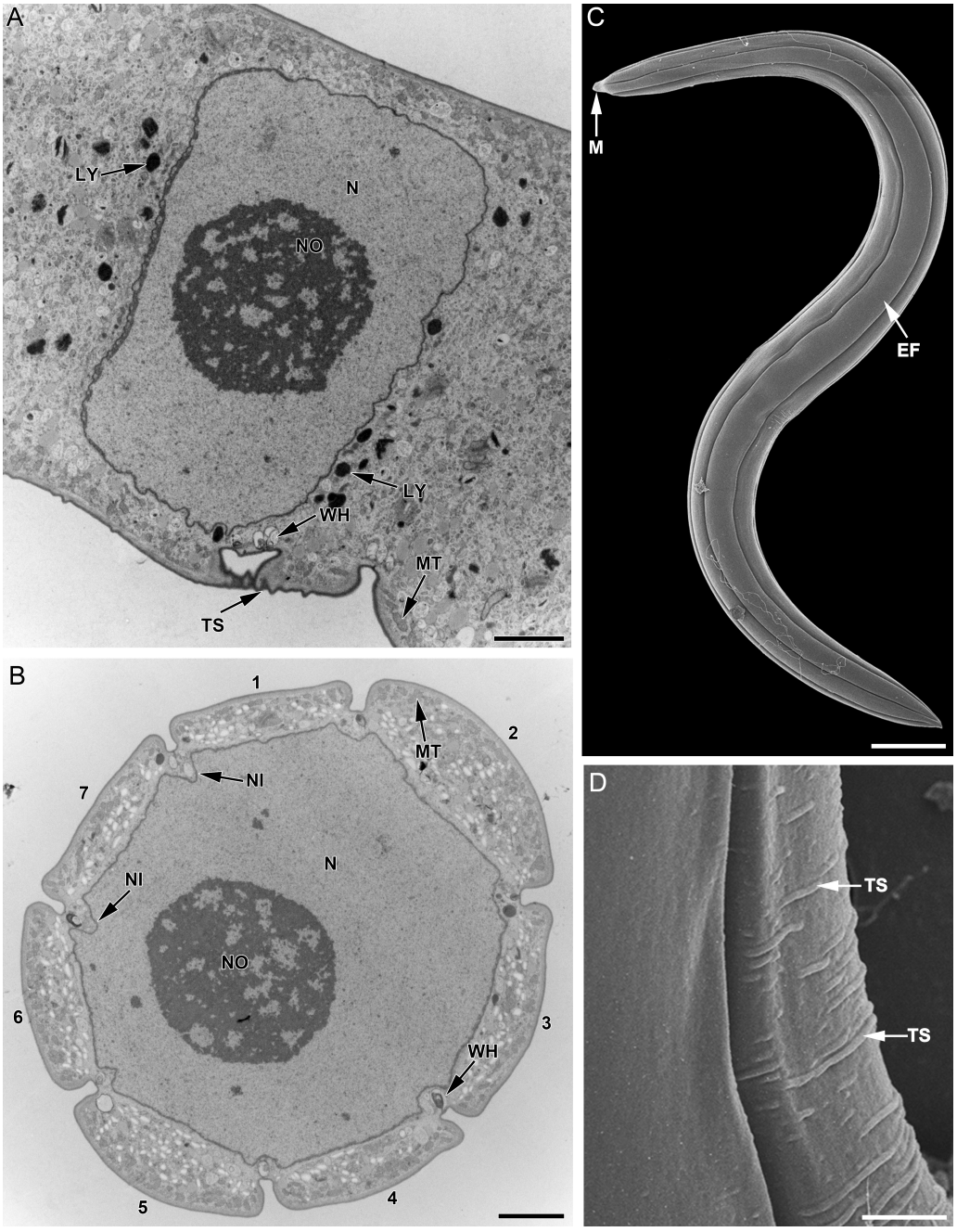

Figure 2. Transmission electron micrographs (TEM) and scanning electron micrographs (SEM) showing the general ultrastructure and surface morphology of the trophozoite stage of *Selenidium terebellae*. **A.** Longitudinal TEM showing the nucleus (N), nucleolus (NO) and transverse striations (TS) on the surface of the cell. The cytoplasm contains mitochondria (MT), pinocytotic whorled vesicles (WH), and putative lysosomes (LY). **B.** Transverse TEM showing the centrally located nucleus (N) and nucleolus (NO). There are seven epicytic folds that correspond with nuclear indentations (NI). The cytoplasm contains mitochondria (MT), and pinocytotic whorled vesicles (WH) positioned beneath the grooves between the epicycitc folds. **C.** SEM showing the general morphology of a trophozoite, the mucron (M), and epicytic folds (EF) that run along the longitudinal axis of the cell. **D.** High-magnification SEM showing transverse striations (TS) on the surface of the cell. Scale bars: A = 2 μm; B = 1 μm; C = 10 μm, D = 3 μm.

The surface of the trophozoites was supported by dense arrays of microtubules, usually in bundles of two to three, that ran under the seven epicytic folds (Fig. 3). Trophozoites also had transverse striations positioned in the middle regions of the cell (Figs 3, 4). Micropores leading to the pinocytotic whorled vesicles were present in the grooves between the epicytic folds, transverse folds and the mucron region (Figs 2A, C; 4A). The mucron region of the trophozoites contained a closed conoid and rhoptry-like vesicles (Figs 4, 5). Alpha-tubulin was localized below the surface of the trophozoite in a pattern corresponding to the subpellicular microtubules and in the mucron region in association with the closed conoid (Figs 5, 6).

Morphology of *Selenidium melongena* n. sp.

The trophozoites were on average 125 μm (range = 30 μm - 155 μm, $n = 57$) long and 30 μm (range = 10 μm - 41 μm, $n = 57$) wide (Fig. 7A-D). The nucleus was located in the center of the trophozoites and was spherical with an average diameter of 15 μm (range = 7 μm - 19 μm, $n = 33$) (Fig. 7A-D). The trophozoites were bottle-shaped or shaped with a rounded posterior end and an anterior end narrowing to a neck-like mucron (Figs 7, 8; Table 1). Cells were light to dark-brown in color from the presence of amylopectin granules. The trophozoites inhabited the coelom of the host and attached to the outside wall of the intestines (Fig. 8). Neither gliding nor bending motility was observed in these trophozoites. The surface of the trophozoites was covered with approximately 30 epicytic folds that were helically arranged and supported by a layer of electron-dense filaments (Figs 8, 9). The mucron region contained an apical cluster of tubule-like material (Fig. 10). Although subpellicular microtubules were not observed, alpha-tubulin was localized in the mucron, corresponding to a conoid, and beneath the entire surface of the trophozoites, corresponding to the overlying pattern of epicytic folds (Fig. 11).

Molecular Phylogenetic Analyses of SSU rDNA Sequences

We generated SSU rDNA sequences from four single-cell isolates for each of the two species, resulting in eight new sequences. Phylogenetic analyses of these SSU rDNA sequences within the context of an alignment encompassing the diversity of apicomplexans demonstrated two highly supported sister clades representing *S. terebellae* and *S. melongena* n. sp., respectively (Fig. 12). The four sequences generated in this study from *S. terebellae* were nearly identical to the previously published sequence from *S. terebellae* (Leander et al. 2003). Intraspecific variation between the four isolates of *M. melongena* n. sp. and *S. terebellae* ranged from 0.11% - 0.60% and 0.11% - 0.37%, respectively. The variation between the two sister clades ranged from 11.7% - 12.8%.

Discussion

Comparative Ultrastructure

The ultrastructure of *S. terebellae* is very similar to other *Selenidium* species examined with TEM; these species have vermiform trophozoites with relatively few epicytic folds supported by layers of microtubules beneath the inner membrane system (Leander 2007; Schrével 1971b; Simdyanov and Kuvardina 2007; Stebbings et al. 1974; Vivier and Schrével 1964). The trophozoites of *Selenidium* species also have transverse striations, bending/twisting motility, and a conoid within the mucron (Leander 2007; Mellor and Stebbings 1980; Schrével 1968, 1971a, b; Simdyanov and Kuvardina 2007; Stebbings et al. 1974; Vivier and Schrével 1964). In this study, the localization of alpha-tubulin throughout the trophozoites of *S. terebellae* provided a straightforward method for visualizing the distribution of subpellicular microtubules and the presence of a conoid. There was some concern about specificity and fixation quality, specifically for the microtubules. However, nonspecific binding in control samples was negligible for both species (Supplementary Material Fig. S1).

The presence of a conoid in *S. terebellae* was inferred previously from SEM images, which demonstrated a cone-shaped mucron and “rhoptry docks” within the tip of the mucron (Leander et al. 2003). Our TEM and immunofluorescence data confirmed this inference. Although we observed a conoid and rhoptries within the mucron, it is unclear from our data if *S. terebellae* also feeds by myzocytosis (Schrével 1968; Simdyanov and Kuvardina 2007). Nonetheless, the TEM data did show evidence for surface-mediated nutrition via rows of micropores and associated pinocytotic whorled vesicles within the grooves between the epicytic folds. This ultrastructural pattern has been observed in other species of *Selenidium*, such as *S. serpulae*, and appears to be a shared trait for the genus (Leander 2007).

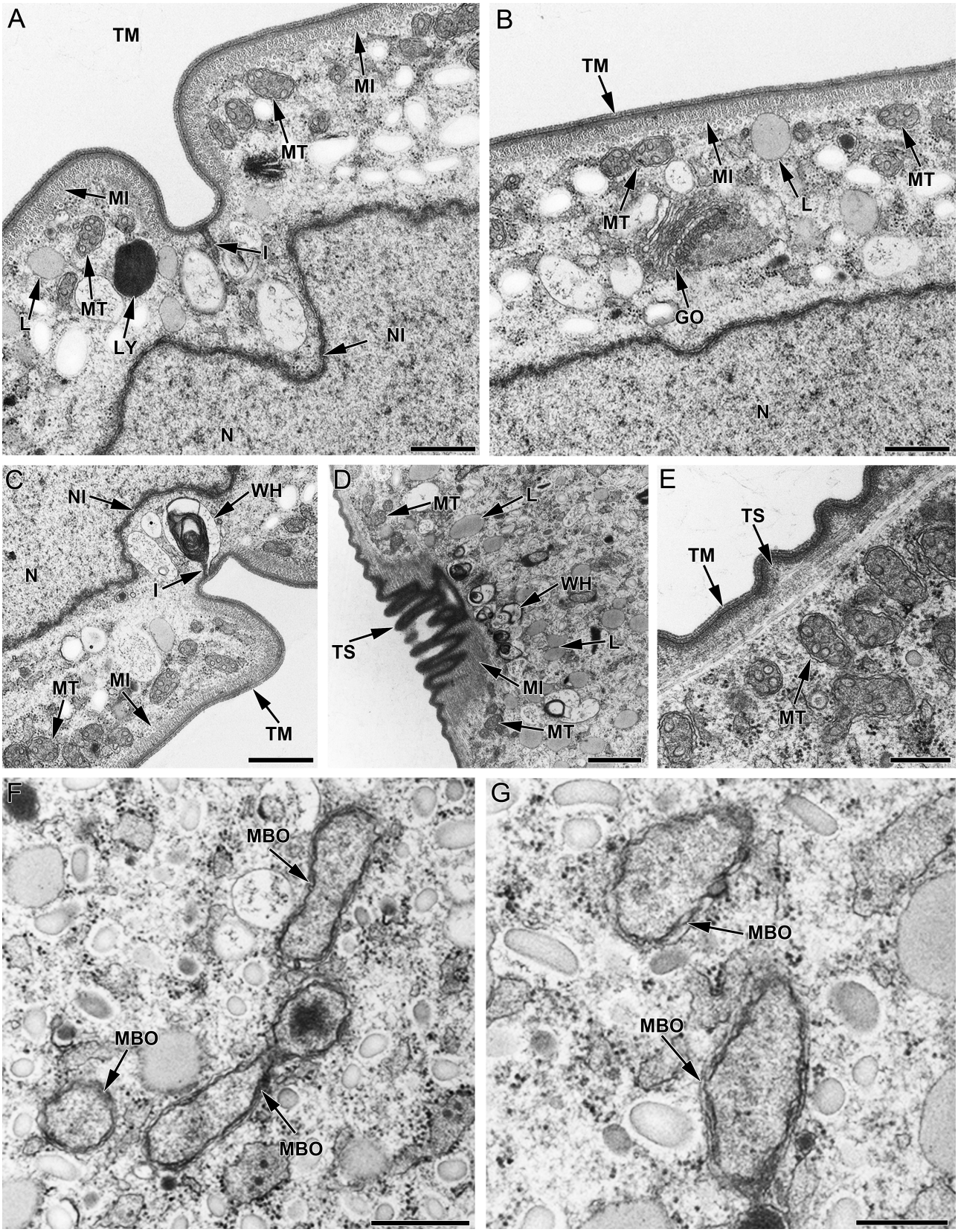
A
TM
MI
MT
MI
I
L
MT
LY
NI
N
B
TM
MI
L
MT
MT
GO
N
C
NI
WH
N
I
MT
MI
TM
D
MT
L
WH
L
TS
MI
MT
E
TS
TM
MT
F
MBO
MBO
MBO
G
MBO
MBO

Figure 3.

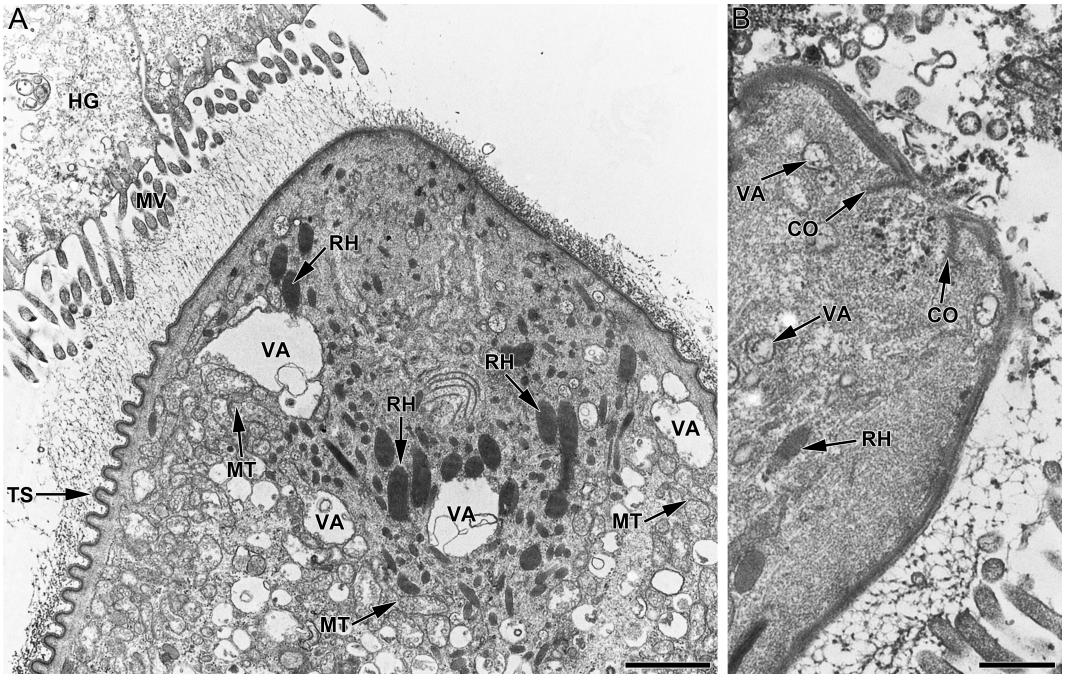

Figure 4. Transmission electron micrographs (TEM) through the mucron region of the trophozoites of *Selenidium terebellae*. **A.** TEM showing host gut cells (HG), host microvilli (MV), and the contents of the mucron. The mucron had transverse striations (TS), rhoptries (RH), mitochondria (MT), and vacuoles (VA). **B**. TEM of the mucron showing the conoid (CO), rhoptries (RH) and vacuoles (VA). Scale bars: A = 5 μm; B = 500 nm.

Four-membrane bound organelles that differed from the pinocytotic whorled vesicles in size, in shape and in having a consistent number of enveloping membranes were also observed throughout the cytoplasm (Fig. 3F-G). Similar organelles were reported in previous ultrastructural studies of *Selenidium* (i.e., *Selenidium pendula*) and strongly resemble the apicoplasts in other lineages of apicomplexans (Hopkins et al. 1999; Köhler 2005; Leander and Ramey 2006; Schrével 1971b; Tomova et al. 2006). These organelles were clustered throughout the cytoplasm within the trophozoites of *S. terebellae*. Because *Selenidium* species are inferred to have retained several ancestral traits in gregarines and perhaps apicomplexans as a whole, an improved understanding of the putative apicoplast in *S. terebellae* using genomic approaches is expected to shed considerable light onto the evolution of this enigmatic organelle.

As detailed in Perkins et al. (2002), a number of other vermiform and archigregarine-like lineages remain to be explored by molecular and/or ultrastructural studies. Future work on *Selenidium*-like gregarines, especially *S. pendula* (the type species), and more enigmatic lineages such as *Selenocystis* (Table 1) will undoubtedly provide deeper insights into the evolution of the archigregarine morphotype and gregarines as a whole.

Figure 3. Transmission electron micrographs (TEM) of the trophozoite stage of *Selenidium terebellae*. **A—C.** Transverse TEM showing microtubules (MI) in layers of two to three under the trilayed membrane complex (TM). The inclusions (I) of micropores were present beneath the grooves between the epicytic folds, and led to the formation of pinocytotic whorled vesicles (WH). The cytoplasm contained lipid droplets (L), putative lysosomes (LY), mitochondria (MT) and Golgi bodies (GO). Nuclear indentations (NI) beneath the grooves between epicytic folds were also visible. **D, E.** Longitudinal TEM showing transverse striations (TS), superficial microtubules (MI), mitochondria with tubular cristae (MT), lipid droplets (L), and pinocytotic whorled vesicles (WH). The outside of the cell was reinforced by a robust trilayed membrane complex (TM). **F—G.** TEM showing organelles (MBO) that are reminiscent of the apicoplasts in other apicomplexans. Scale bars: A—D = 500 nm; D = 1 μm; E = 500 nm; F—G = 500 nm.

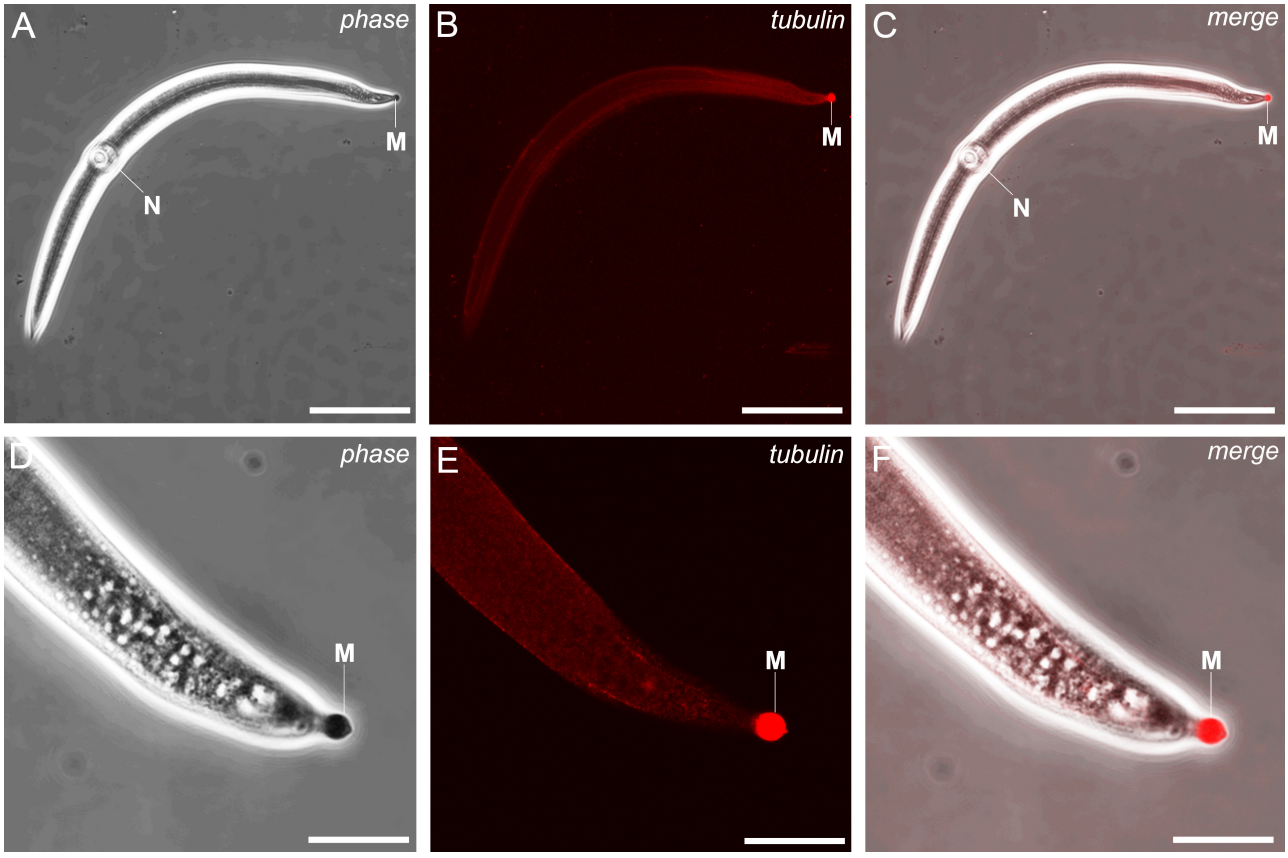

Figure 5. Confocal images of the trophozoite of *Selenidium terebellae*. **A—F.** Phase contrast (*phase*), alpha-tubulin (*tubulin*) and merged (*merge*) images showing the localization of alpha-tubulin throughout the trophozoite and the mucron.

Justification of *Selenidium melongena* n. sp.

The trophozoites of this new species were very different from those in other gregarine species described previously. *S. melongena* n. sp. has trophozoites with 30 to 40 epicytic folds that were helically arranged along the longitudinal axis of the cell. No movement (e.g., gliding motility) or changes in cell shape were observed in this species. TEM images showed that the epicytic folds are supported by arrays of fibrils rather than microtubules per se. These fibrils were more reminiscent of the subpellicular networks described as transverse fibrils by MacMillan (1973) in *Nematocytis magna* or the filamentous myonemes seen in *Gregarina polymorpha* (Heintzelman 2004); other studies have reported networks of fibrils (myonemes) underlying eugregarines in terrestrial hosts (Hildebrand 1980; Ormieres and Daumal 1970; Valigurová et al. 2013). Further molecular phylogenetic work will be necessary to evaluate the level of homology of these structures in lineages for which the current relationships are unclear.

Although microtubules were not observed, the alpha-tubulin immunofluorescence data indicated a tubulin-based scaffold localized just below the surface of the helical folds. The alpha-tubulin immunofluorescence data also showed that an apical cluster of tubule-like elements was present within the mucron. These data also demonstrate how immunofluorescence approaches offer another way to detect the presence of a conoid and other tubulin-based structures in gregarine trophozoites, which would otherwise need to be tediously sectioned for TEM (see Heintzelman 2004; Kuriyama et al. 2005; Valigurová 2012). Future work using immunofluorescence approaches on other gregarine lineages that have been inferred to possess ancestral traits (e.g., *Veloxidium*) will enhance our ability to

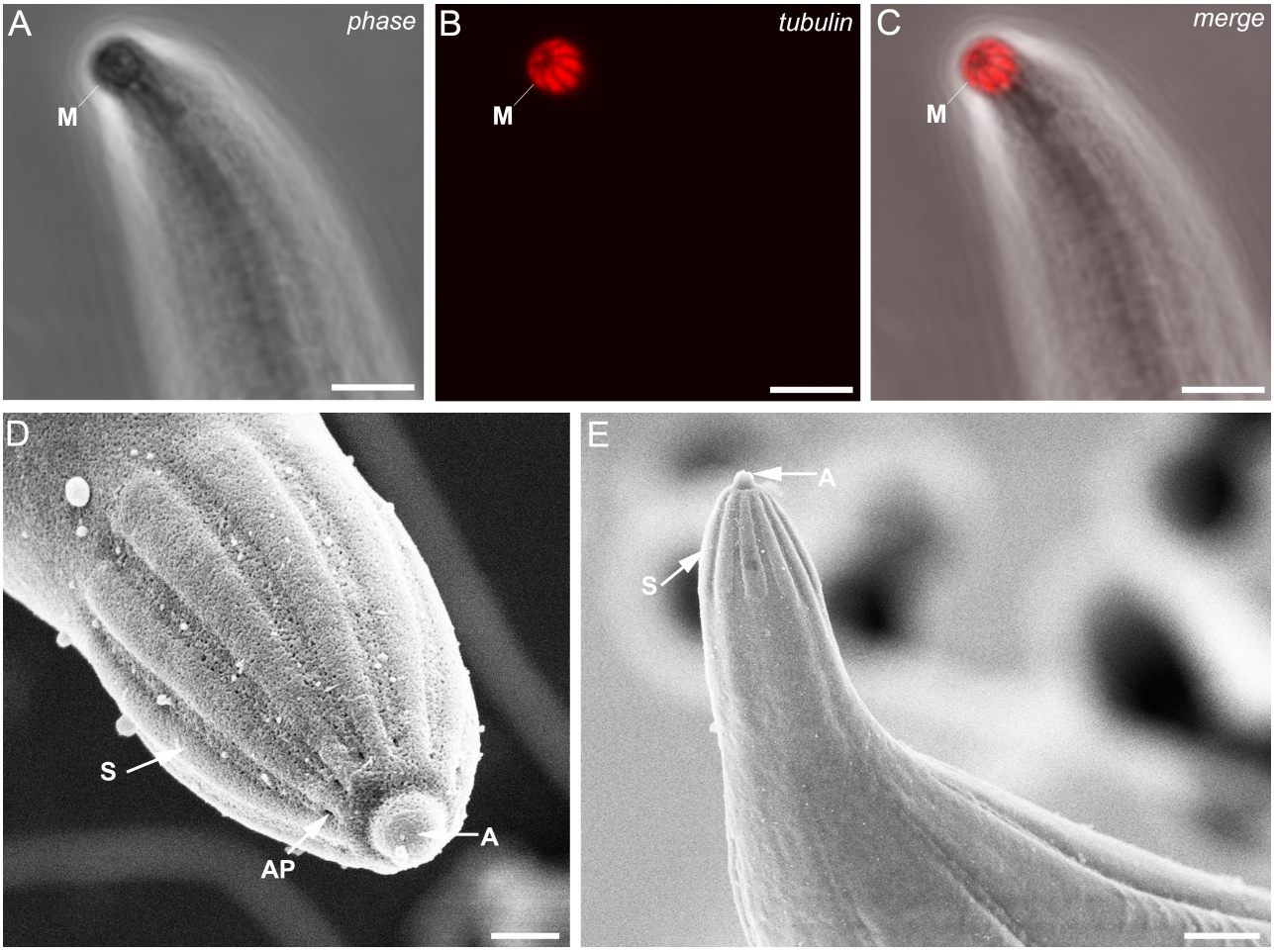

Figure 6. High-magnification confocal and scanning electron micrographs of *Selenidium terebellae* Ray 1930 showing ten distinct longitudinal striations (S), an "apical tip" (A) and apical pores (AP) located within the anterior end of the grooves between the striations. Scale bars: A—C = 1 μm; D = 500 nm; E = 1 μm.

study character evolution within *Selenidium* and beyond.

The only gregarine species we could find in the literature with trophozoites that are vaguely similar to those in *S. melongena* n. sp. is *Merogregarina amaroucii* Porter, 1908, which was isolated from the intestines of an ascidian host. The trophozoites of *M. amaroucii* have an overall shape that is similar to *S. melongena* n. sp., but there is no mention of helically arranged epicytic folds in the original description (Porter 1908). The five to seven epicytic folds that were reported in *M. amaroucii* were restricted to the anterior region of the cell (Perkins et al. 2002; Porter 1908). This, along with the fact that *M. amaroucii* was isolated from an ascidian, suggest that *S. melongena* n. sp. and *M. amaroucii* are two different species of marine gregarines; ultrastructural and molecular data from *M. amaroucii* would be necessary to evaluate this relationship further.

Niche Partitioning in Gregarine Apicomplexans

The molecular phylogenetic analyses demonstrated a close sister relationship between *S. terebellae* and *S. melongena* n. sp., which reflects a pattern of morphological divergence that would otherwise be undetectable from comparative morphology alone. *S. terebellae* has a set of molecular, morphological and motility traits inferred to be ancestral for gregarines, such as trophozoites with a conoid, a small number of longitudinal epicytic folds, dense layers of microtubules beneath the cell surface, and bending/twisting movement. Collectively, these characteristics convey the contemporary archigregarine concept (Leander 2008;

Figure 7. Differential interference contrast (DIC) light micrographs showing the general morphology of the trophozoite stage of *Selenidium melongena* n. sp. The mucron is oriented towards the top of the figures. **A**. One cell imaged at two different focal planes. **A—D.** The nucleus (N) is centrally located, and a sheath of host material (arrow) is visible on some of the trophozoites. Scale bar: 15 μm.

Schrével 1971a; Wakeman and Leander 2012). By contrast, the trophozoites of *S. melongena* n. sp. have traits that are more consistent with species of marine eugregarines like lecudinids and urosporids than with *Selenidium* (Leander 2008; Leander et al. 2003; Rueckert et al. 2010; Schrével 1971b; Wakeman and Leander 2012). The trophozoites of this species were non-motile and lacked the robust arrays of microtubules beneath the cell surface, although the immunofluorescence data still support the existence of a tubulin-based framework that, in addition to other subpellicular fibrous elements, may support the helically arranged epicytic folds and a conoid-like scaffold within the mucron.

The distinct morphological differences between these two closely related gregarine species are correlated with two different locations within the polychaete host: *S. terebellae* infects the intestinal lumen, and *S. melongena* n. sp. was predominately observed attached to the outer intestinal wall. The molecular and morphological data combined suggest that this pattern of morphological divergence is associated with niche partitioning within the host. Other coelomic gregarines like *Lithocystis*, *Urospora* and *Pterospora* have a wide variety of surface morphology, ranging from folds to bumps and ridges (Coulon and Jangoux 1987; Landers and Leander 2005; Leander 2008). One of the features that these gregarines share is a motility pattern of dynamic surface undulations (Leander et al. 2006). Molecular phylogenetic data demonstrate that *Lithocystis*, *Urospora* and *Pterospora*, although found in distantly related hosts (holothuroideans and maldinid polychaetes), are part of a diverse monophyletic group that also contains marine lecudinids (Leander et al. 2006; Rueckert and Leander 2009; Wakeman and Leander 2012). *Selenidium melongena* n. sp. has a helical pattern of epicytic folds on the surface of the trophozoites, but the cell membrane does not pulsate like *Lithocystis*, *Urospora* and *Pterospora*. This suggests that there is a fundamental difference in how *S. melongena* n. sp and urosporid coelomic gregarines acquire nutrients. Our observations from combined SEM, TEM and confocal micrographs of *S. melongena* n. sp. suggest that the conoid-like cluster of tubulin-based elements at the anterior of the trophozoite stage enable this parasite to penetrate the outer intestinal wall of its host in order to feed, presumably, via myzocytosis; a strategy of acquiring nutrients known in other species of *Selenidium*.

Although one way to distinguish some gregarine species is by their host affiliation, there are still many examples of different gregarine species that occupy the same host (Coulon and Jangoux 1987; Levine 1971; Rueckert and Leander 2009; Wakeman and Leander 2013a, b). For example, Coulon and Jangoux (1987) reported on five species of gregarines co-infecting one species of

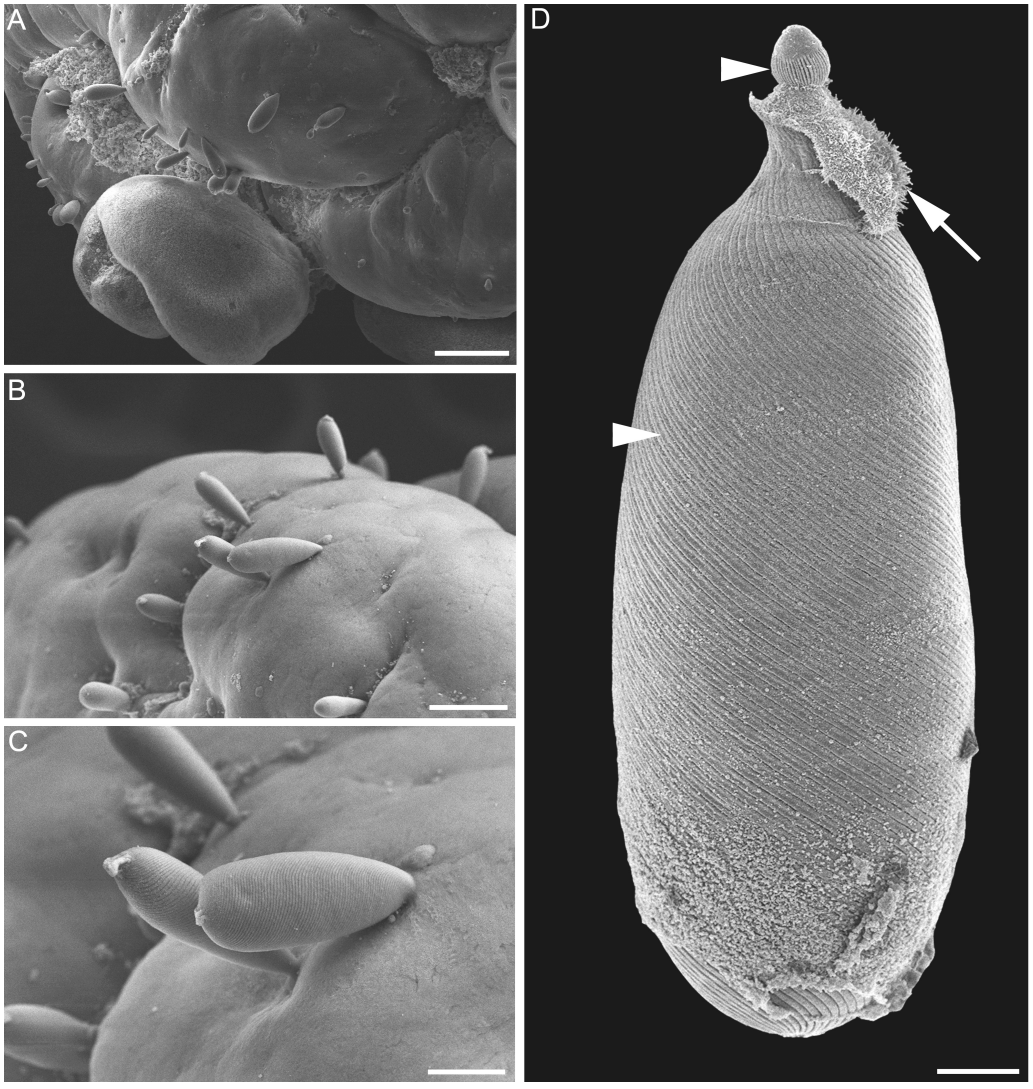

Figure 8. Scanning electron micrographs (SEM) of *Selenidium melongena* n. sp. showing the general morphology of the trophozoites and their attachment to the outside surface of the host intestine. **A—C.** Low-magnification SEM showing the distribution and attachment of trophozoites on the outside surface of the gut. **D.** SEM showing the general morphology of the trophozoite with the mucron oriented upwards. A sheath of host gut material (arrow) was still present around the mucron. Epicytic folds (arrowheads) were present on the mucron, and spiraled in a helical arrangement over the entire surface of the cell. Scale bars: A = 100 μm; B = 80 μm; C = 25 μm D = 10 μm.

echinoderm. Some of these host-parasite relationships have been shown to be highly specific to even certain life stages of the host. For instance, four species of *Gregarina* specialize on either adult or larval stages of a single species of arthropod (Clopton et al. 1992; Clopton and Janovy 1993). In these cases, the use of molecular data is extremely important for understanding the boundaries between species and their interrelationships where morphology alone may be insufficient, and subsequently misleading. The data we report here from *S. terebellae* and *S. melongena* n. sp. demonstrates a novel case of morphological divergence in two unanticipated sister species.

Taxonomic Description

Phylum Apicomplexa Levine, 1970
Gregarinea Bütschli, 1882, stat. nov. Grassé, 1953
Order Eugregarinorida Léger, 1900
Selenididae Brasil, 1907
Selenidium Giard, 1884

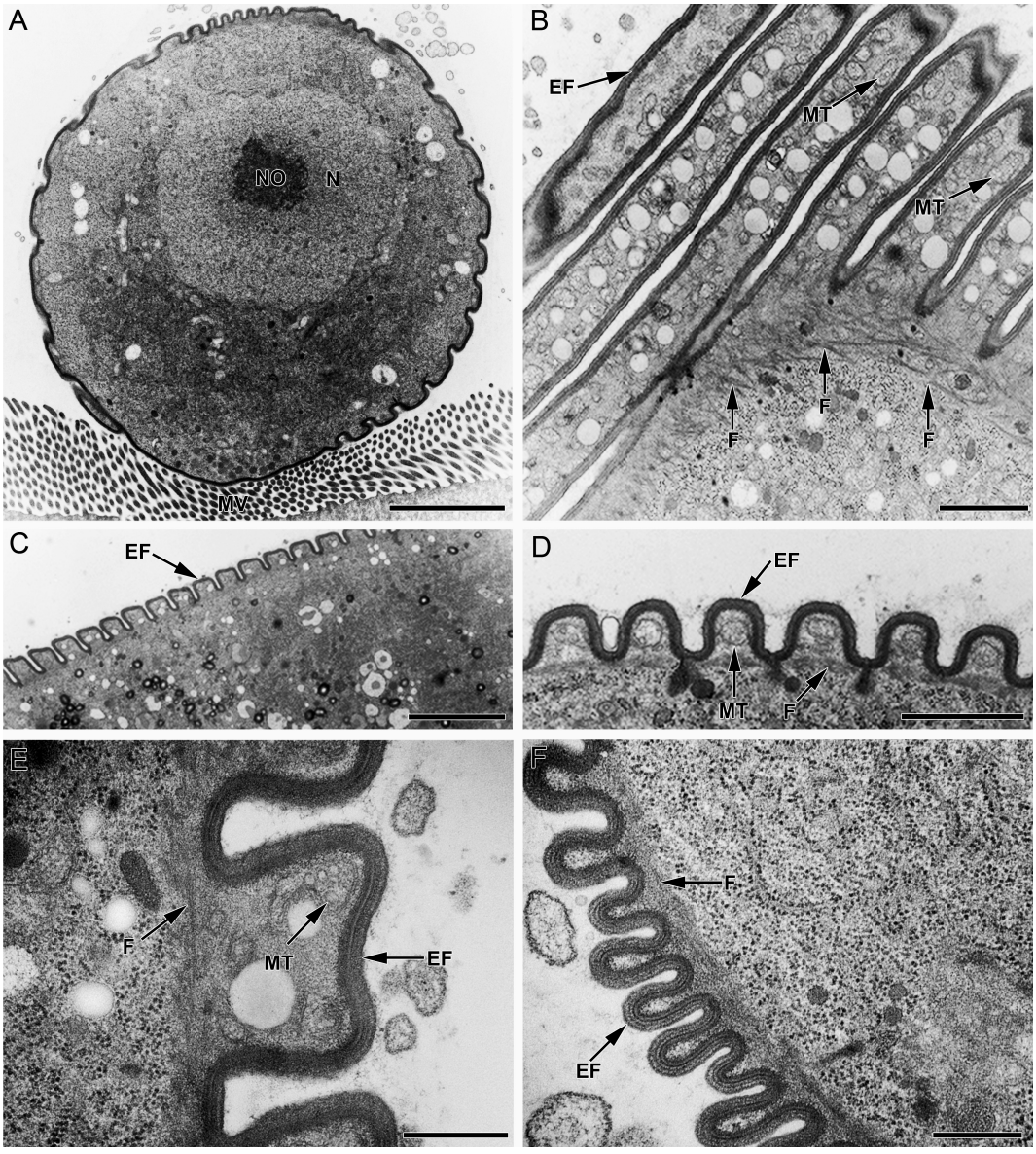

Figure 9. Transmission electron micrographs (TEM) showing the general ultrastructure of trophozoite stages of *Selenidium melongena* n. sp. **A.** Transverse TEM showing the nucleus (N), nucleolus (NO), and host microvilli (MV) **B.** Tangential TEM showing the trilayered membrane of the helically arranged epicytic folds, mitochondria (MT) and fibrils (F). **C.** Longitudinal TEM image showing epicytic folds (EF) and a general view of the cytoplasm of the trophozoite. **D.** Transverse TEM image through the epicytic folds (EF) showing fibrils (F) and mitochondria (MT) with tubular cristae positioned under each fold. **E—F.** TEM images through the pellicle of a trophozoite showing epicytic folds (EF) in the trilayered pellicle (TM), mitochondria (MT) and fibrils (F). Scale bars: A. = 3 μm; B = 1.5 μm; C, D = 2 μm; E = 0.5 μm; F = 0.5 μm.

Selenidium melongena Wakeman, Heintzelman and Leander n. sp.

Description: Trophozoites light to dark-brown, bottle-shaped or shaped with a rounded posterior end and a narrow, neck-like mucron. Trophozoite surface with approximately 30 epicytic folds arranged in a helical pattern. Trophozoites averaged 125 μm in length and 30 μm in width. Mucron contains an apical cluster of tubular elements. Trophozoites without gliding motility or bending movement.

DNA sequence: Small subunit rDNA (Genbank Accession KC890799).

Type micrograph: Fig. 7D

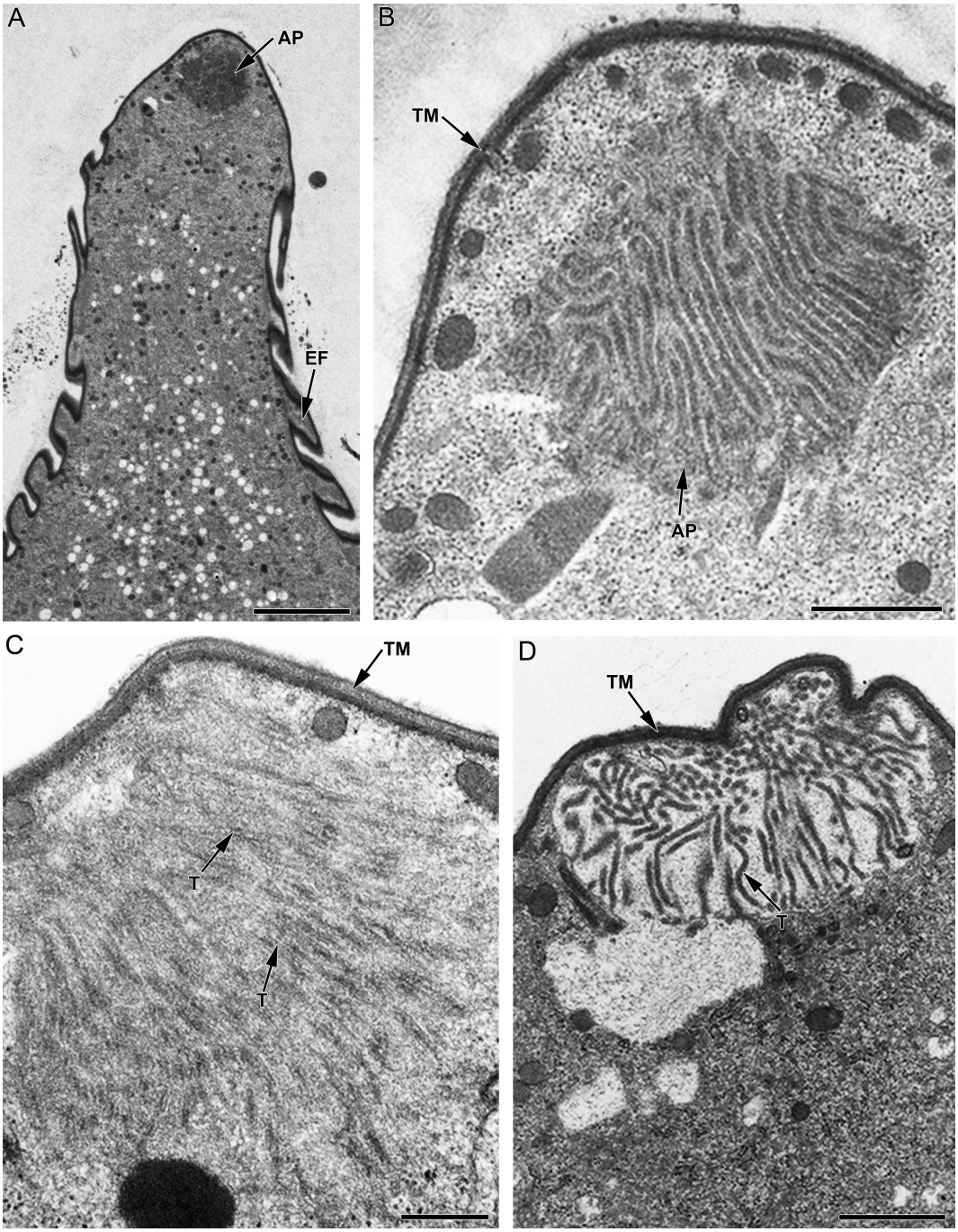

Figure 10. Transmission electron micrographs (TEM) of longitudinal sections through the mucron region of *Selenidium melongena* n. sp. **A—D.** TEM showing epicytic folds (EF), the trilayered membrane (TM), and an apical cluster (AP) of tubular material (T). Scale bars: A = 2 μm; B,C = 500 nm; D = 1 μm.

Syntype: Parasites on gold sputter-coated SEM stubs have been deposited in the Beaty Biodiversity Museum (Marine Invertebrate Collection) at the University of British Columbia, Vancouver, Canada. Museum Code – MI-PR127. Resin blocks and fixed slides containing infected gut material and/or individual trophozoites are held under the same code.

Type host: *Thelepus japonicus* Marenzeller 1884.

Location within host: Coelom, attached to outer wall of intestine.

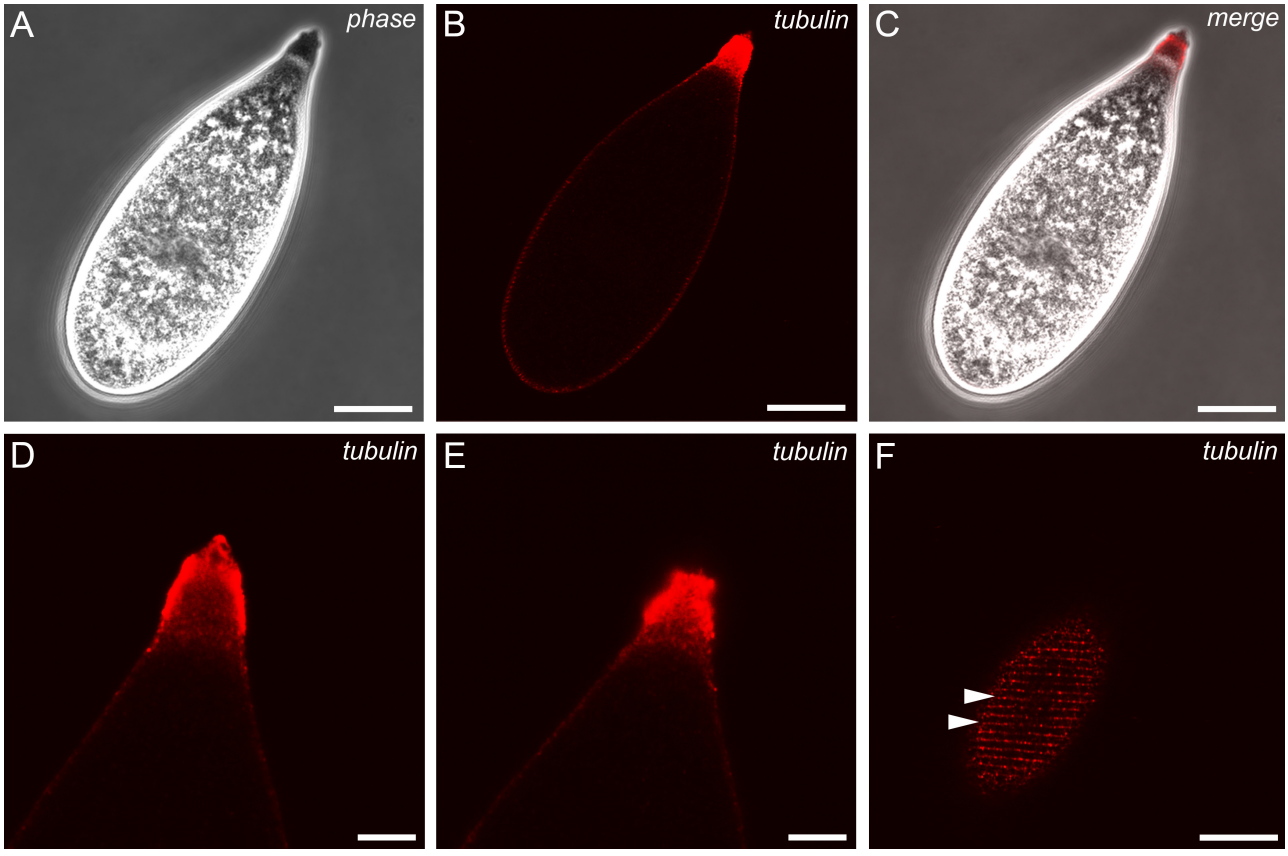

Figure 11. Confocal and phase contrast images showing the localization of alpha-tubulin (*tubulin*) in the trophozoites of *Selenidium melongena* n. sp. **A—C.** Confocal and phase contrast images showing the localization of alpha-tubulin within the enitre cell. **D—E.** Confocal images showing the localization of alpha-tubulin (*tubulin*) within the mucron. **F.** Confocal image showing the localization of alpha-tubulin (*tubulin*) within the helically arranged epicytic folds (arrowheads). Scale bars: A-C, F = 10 μm; D-E = 5 μm.

Type locality: Low intertidal to subtidal zone (<5 m) at Clover Point, Victoria, British Columbia, Canada (48°24′11.36′ N 123°21′01.94″ W).

Etymology: The epithet "*melongena*" stems from the Latin, meaning "eggplant", and refers to the shape of the trophozoites.

Methods

Collection of organisms: *Thelepus japonicus* Marenzeller, 1884 was collected in January 2013 under rocks in the low intertidal to sub tidal zone while SCUBA diving at a depth < 5 m near Clover Point 48°24′11.36″ N 123°21′01.94″ W, Victoria, British Columbia, Canada. Host material was stored in containers of seawater on ice for 24 hours prior to dissection. The complete gut was removed from the host using fine forceps. Some of the whole gut material was prepared for SEM and TEM. Other gut material was teased apart with fine forceps on well slides to release trophozoites that were individually isolated for light microscopy, SEM, TEM and DNA extraction.

Light microscopy: Hand-drawn glass pipettes were used to isolate and clean individual trophozoites using an inverted microscope (Zeiss Axiovert 200, Carl-Zeiss, Göttingen, Germany) attached to a PixeLink Megapixel color digital camera

Figure 12. Maximum likelihood (ML) tree derived from phylogenetic analyses of the 84-taxon dataset (1,072 unambiguously aligned sites) of small subunit (SSU) rDNA sequences. This tree was inferred using the GTR + I + Γ substitution model (-lnL = 18,398.84797, gamma shape = 0.5710, proportion of invariable sites = 0.1940). Bootstrap support values are listed above Bayesian posterior probabilities. Black dots on branches denote bootstrap support values and Bayesian posterior probabilities of 95/0.95 or greater, respectively. Bootstrap and Bayesian values less than 55 and 0.95, respectively, were not added to this tree. Four single-cell isolations each from *Selenidium melongena* n. sp. and *Selenidium terebellae* are highlighted in grey boxes. Some branches were shortened by multiples of the length of the substitutions/site scale bar.

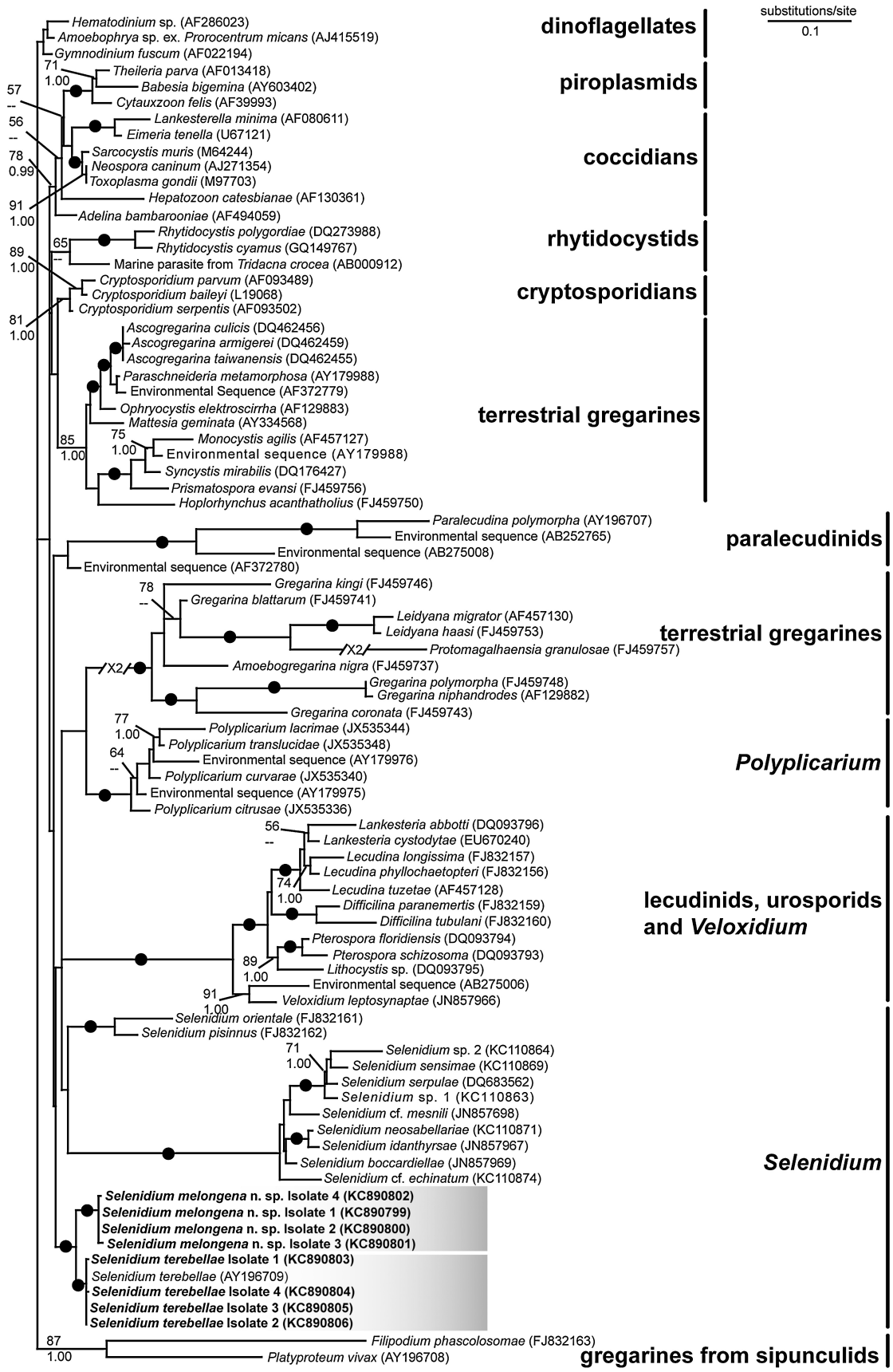
substitutions/site
0.1
dinoflagellates
piroplasmids
coccidians
rhytidocystids
cryptosporidians
terrestrial gregarines
paralecudinids
terrestrial gregarines
Polyplicarium
lecudinids, urosporids and Veloxidium
Selenidium
gregarines from sipunculids
Hematodinium sp. (AF286023)
Amoebophrya sp. ex. Prorocentrum micans (AJ415519)
Gymnodinium fuscum (AF022194)
Theileria parva (AF013418)
Babesia bigemina (AY603402)
Cytauxzoon felis (AF39993)
Lankesterella minima (AF080611)
Eimeria tenella (U67121)
Sarcocystis muris (M64244)
Neospora caninum (AJ271354)
Toxoplasma gondii (M97703)
Hepatozoon catesbianae (AF130361)
Adelina bambarooniae (AF494059)
Rhytidocystis polygordiae (DQ273988)
Rhytidocystis cyamus (GQ149767)
Marine parasite from Tridacna crocea (AB000912)
Cryptosporidium parvum (AF093489)
Cryptosporidium baileyi (L19068)
Cryptosporidium serpentis (AF093502)
Ascogregarina culicis (DQ462456)
Ascogregarina armigerei (DQ462459)
Ascogregarina taiwanensis (DQ462455)
Paraschneideria metamorphosa (AY179988)
Environmental Sequence (AF372779)
Ophryocystis elektroscirrha (AF129883)
Mattesia geminata (AY334568)
Monocystis agilis (AF457127)
Environmental sequence (AY179988)
Syncystis mirabilis (DQ176427)
Prismatospora evansi (FJ459756)
Hoplorhynchus acanthatholius (FJ459750)
Paralecudina polymorpha (AY196707)
Environmental sequence (AB252765)
Environmental sequence (AB275008)
Environmental sequence (AF372780)
Gregarina kingi (FJ459746)
Gregarina blattarum (FJ459741)
Leidyana migrator (AF457130)
Leidyana haasi (FJ459753)
Protomagalhaensia granulosae (FJ459757)
Amoebogregarina nigra (FJ459737)
Gregarina polymorpha (FJ459748)
Gregarina niphandrodes (AF129882)
Gregarina coronata (FJ459743)
Polyplicarium lacrimae (JX535344)
Polyplicarium translucidae (JX535348)
Environmental sequence (AY179976)
Polyplicarium curvarae (JX535340)
Environmental sequence (AY179975)
Polyplicarium citrusae (JX535336)
Lankesteria abbotti (DQ093796)
Lankesteria cystodytae (EU670240)
Lecudina longissima (FJ832157)
Lecudina phyllochaetopteri (FJ832156)
Lecudina tuzetae (AF457128)
Difficilina paranemertis (FJ832159)
Difficilina tubulani (FJ832160)
Pterospora floridiensis (DQ093794)
Pterospora schizosoma (DQ093793)
Lithocystis sp. (DQ093795)
Environmental sequence (AB275006)
Veloxidium leptosynaptae (JN857966)
Selenidium orientale (FJ832161)
Selenidium pisinnus (FJ832162)
Selenidium sp. 2 (KC110864)
Selenidium sensimae (KC110869)
Selenidium serpulae (DQ683562)
Selenidium sp. 1 (KC110863)
Selenidium cf. mesnili (JN857698)
Selenidium neosabellariae (KC110871)
Selenidium idanthyrsae (JN857967)
Selenidium boccardiellae (JN857969)
Selenidium cf. echinatum (KC110874)
Selenidium melongena n. sp. Isolate 4 (KC890802)
Selenidium melongena n. sp. Isolate 1 (KC890799)
Selenidium melongena n. sp. Isolate 2 (KC890800)
Selenidium melongena n. sp. Isolate 3 (KC890801)
Selenidium terebellae Isolate 1 (KC890803)
Selenidium terebellae (AY196709)
Selenidium terebellae Isolate 4 (KC890804)
Selenidium terebellae Isolate 3 (KC890805)
Selenidium terebellae Isolate 2 (KC890806)
Filipodium phascolosomae (FJ832163)
Platyproteum vivax (AY196708)

Figure 12.

(PL-A662-KIT, Ottawa, Canada). Some isolates were photographed on well slides, washed in autoclaved, filtered seawater and collected for DNA extraction and single-cell PCR amplification (SC-PCR). Isolated trophozoites were also photographed with differential interference contrast (DIC) using a Leica DC 500 color camera attached to a Zeiss Axioplan 2 microscope (Carl-Zeiss, Göttingen, Germany).

Immunolocalization and confocal microscopy: Trophozoites of *S. terebellae* and *S. melongena* n. sp. were isolated from the host and washed at least twice (or until clean) in chilled, filtered seawater. Isolates were initially fixed for 5 minutes in 4% paraformaldehyde in PBS containing 50 mM K-EGTA (Heintzelman 2004). Isolates were washed three times with PBS/K-EGTA and permeabilized for 30 minutes in PBS/K-EGTA containing 0.1% BSA and 0.1% Triton X-100. Cells were then incubated overnight with a polyclonal alpha-tubulin primary antibody: Anti-alpha tubulin from chicken Cat no. SAB3500023-100UG (Sigma-Aldrich, Ontario, Canada). Cells were then washed four times in PBS/K-EGTA containing 0.1% BSA and 0.1% Triton X-100, and incubated for five hours with a secondary antibody: AlexaFluor (R) 568 Goat A anti-chicken IgG Cat. no. A11041 (Molecular Probes, Eugene, Oregon). Controls were made for each species by following this procedure; however, the primary antibody was not added to the control samples. Specimens where then mounted on glass slides and sealed with fingernail polish, and images acquired using an Olympus FV10i Confocal microscope (Olympus, Tokyo, Japan). Control samples showed that both the autofluorescence of the specimens and non-specific binding of the secondary antibody was negligible (Supplementary Material Fig. S1). Fixation was also performed for 5 min with methanol at -20 °C. Samples were washed, permeabilized and stained in the same manner as described for paraformaldehyde fixation. These samples had a similar staining pattern as the samples fixed with paraformaldehyde. However, the paraformaldehyde-fixed samples were chosen as representative, based on the quality of the background and lack of debris covering the cells.

Scanning electron microscopy: Individual trophozoites were pooled in 2% glutaraldehyde in seawater on ice. A 10 μl polycarbonate membrane filter was placed within a Swinnex filter holder (Millipore Corp. Billerica, MA, USA). Trophozoites were filtered onto the membrane using a syringe with distilled water, and the holder was placed in a small beaker (4 cm diam. and 5 cm tall) that was filled with distilled water. Ten drops of 1% OsO_4 were added to the opening of the filter holder, and the samples were post-fixed on ice for 30 minutes. The syringe was used to slowly run distilled water over all samples. A graded series of ethanol washes (30%, 50%, 75%, 85%, 95% and 100%) was then used to dehydrate the fixed cells using the syringe system. Following dehydration, the polycarbonate membrane filters containing the trophozoites were transferred from the Swinnex filter holders into an aluminum basket submerged in 100% ethanol in preparation for critical point drying with CO_2. The dried polycarbonate membrane filters containing the trophozoites were mounted on aluminum stubs, sputter coated with 5 nm gold and viewed with a Hitachi S4700 scanning electron microscope (Nissei Sangyo America, Ltd., Pleasanton, CA). Some SEM data were presented on a black background using Adobe Photoshop 6.0 (Adobe Systems, San Jose, California).

Transmission electron microscopy: Single trophozoites of *S. terebellae* and *S. melongena* n. sp. as well as small sections (5 mm) of host gut tissue were collected for TEM in Eppendorf Tubes. Initially, these preparations were fixed in 2.5% glutaraldehyde in seawater on ice for 30 minutes. After being washed three times with cacodylate buffer (0.2 M pH 7.2), the material was post-fixed in 1% OsO_4 in cacodylate buffer for 90 minutes. Following this fixation period, cells were washed three times with cacodylate buffer and suspended in ~1.5% low melting point agarose (temperature ~37 °C). The cell/agarose solutions were placed on ice for two to three minutes to solidify. The agarose containing the cells and sections of gut tissue was then removed from the tube and regions of the agar with trophozoites were excised using a razor blade under a stereo microscope (LeicaL2, Wetzlar, Germany). These chunks of agar were placed in an Eppendorf tube and dehydrated through a graded series of ethanol washes (70%, 80% 85%, 90%, 95%, 100%, 100%, 100%), lasting five minutes each. The material was then placed in a 1:1 mixture of ethanol and acetone, and 100% acetone for five minutes. Cells were embedded in 1:1 acetone and Epon 812 resin for 30 minutes, and then transferred to 100% resin overnight. After changing the 100% resin one time, material was polymerized for 32 hours at ~ 68 °C. Ultrathin sections were cut using a diamond knife on a Leica EM UC6 ultra-microtome and double-stained with 2% (w/v) uranyl acetate and lead citrate. Sections were observed using a Hitachi H7600 electron microscope.

DNA extraction, amplification and sequencing: Individual trophozoites were placed in a 1.5 ml Eppendorf tube containing cell lysis buffer. Genomic DNA was extracted with the standard protocol provided by the MasterPure complete DNA & RNA purification kit (Epicentre Biotechnologies, Madison, WI, USA). However, the final elution step was lowered to 4 μl, with the goal of concentrating extracted DNA prior to SC-PCR amplification. Outside primers, PF1 5′ – GCGCTACCTGGTTGATCCTGCC – 3′ and SSUR4 5′ – GATCCTTCTGCAGGTTCACCTAC – 3′ (Leander et al. 2003), were used in a 25 μl PCR with EconoTaq 2X Master Mix (Lucigen Corp., Middleton, WI, USA). The following program was used on the thermocycler for the initial amplification: Initial denaturation at 94 °C for 2:00 m; 35 cycles of denature at 94 °C for 0:30 s, anneal at 52 °C for 0:30 s, extension at 72 °C for 1:50 m., final extension 72 °C 9:00 m. Subsequently, internal primers F2 5′ – GGTAGYGACAAGAAATAACAAC – 3′ and R2 5′ – GAYTACGACGGTATCTGATCGTC – 3′ (Wakeman and Leander 2013b) were paired with outside primers in a nested PCR using the following program on a thermocycler: Initial denaturation for 94 °C for 2:00 m; 25 cycles of denature at 94 °C for 0:30 s., anneal at 55 °C for 0:30 s., extension at 72 °C for 1:30 m.; final extension at 72 °C for 9:00 m. All SC-PCR products (~1,200 bp and 1,000 bp for F2-SSUR4 and R2-PF1, respectively) were separated on agarose gels and isolated using the UltraClean15 DNA Purification Kit (MO BIO, Laboratories, Inc., Carlsbad, CA, USA), and cloned into a pCR 2.1 vector using a StrataClone PCR cloning kit (Agilent Technologies, Santa Clara, CA, USA). Sixteen clones from each cloning reaction were screened for size, digested with HaeIII restriction enzyme (Invitrogen, Frederick, MD, USA) and sequenced using vector primers and ABI Big-dye reaction mix. Novel sequences (~1,750 bp) were identified using the National Center for Biotechnology Information's (NCBI) BLAST tool, confirmed with molecular phylogenetic analyses, and deposited into GenBank (KC890799-KC890806).

Molecular phylogenetic analyses: We constructed a comprehensive 84-taxon alignment (1,072 unambiguously aligned sites) containing SSU rDNA sequences from the eight single-cell isolates of *S. terebellae* and *S. melongena* n. sp., as well as three dinoflagellate sequences (outgroup), and 73 sequences representing the major apicomplexan subclades. The alignment was initially constructed using MUSCLE (Edgar 2004) and was subsequently edited and fine-tuned using MacClade 4.08

(Maddison and Maddison 2005); gaps and ambiguously aligned regions were excluded from the analyses.

Jmodeltest 0.1.1 selected a GTR + I + Γ model of evolution under Akaike Information Criterion (AIC) and AIC with correction (AICc) (proportion of invariable sites = 0.1940, gamma shape = 0.5710 (Posada and Crandall 1998). Garli0.951-GUI (www.bio.utexas.edu/faculty/antisense/garli/Garli.html) was used to infer a maximum likelihood (ML) tree and for ML bootstrap analyses (500 pseudoreplicates, one heuristic search per pseudoreplicate) (Zwickl 2006).

Bayesian posterior probabilities were calculated using the following parameters on the program MrBayes 3.1.2. (Huelsenbeck and Ronquist 2001; Ronquist and Huelsenbeck 2003): [GTR (Lset nst = 6); gamma distribution (of rate among sites] and Monte Carlo Markov Chains [starting trees = 4; default temperature = 0.2; generations = 7,500,000; sample frequency = 100; prior burn-in = 750,000 trees]; stop rule of 0.01 (i.e. when the average split deviation fell below 0.01, the program would terminate)]. Burn-in was confirmed manually, and majority-rule consensus trees were constructed; posterior probabilities correspond to the frequency at which a given node is found in the post-burn-in trees. PAUP 4.0 (Swofford 1999) was used to calculate percent differences between the SSU rDNA sequences of both isolates. The alignment use in this study is available from the authors by request.

Acknowledgements

This research was supported by grants to BSL from the National Science and Engineering Research Council of Canada (NSERC 283091-09) and the Canadian Institute for Advanced Research, Program in Integrated Microbial Biodiversity.

Appendix A. Supplementary data

Supplementary data associated with this article can be found, in the online version, at http://dx.doi.org/10.1016/j.protis.2014.05.007.

References

Adl SM, Simpson AGB, Lane CE, Lukes J, Bass D, et al. (2012) The revised classification of eukaryotes. J Eukaryot Microbiol **59**:429–493

Clopton RE, Janovy J (1993) Developmental niche structure in the gregarine assemblage parasitizing *Tenebrio molitor*. J Parasitol **79**:701–709

Clopton RE, Janovy J, Percival TJ (1992) Host stadium specificity in the gregarine assemblage parasitizing *Tenebrio molitor*. J Parasitol **78**:334–337

Coulon P, Janoux M (1987) Gregarine species (Apicomplexa) parasitic in the burrowing echinoid *Echinocardium cordatum*: occurrence and host reaction. Dis aquat Org **2**:135–145

Cox FEG (1994) The evolutionary expansion of the Sporozoa. Int J Parasitol **24**:1301–1316

Dyson J, Grahame J, Evennett PJ (1993) The mucron of the gregarine *Digyalum oweni* (Protozoa, Apicomplexa), parasitic in littorina species (Mollusca, Gastropoda). J Nat His **27**:557–564

Dyson J, Grahame J, Evennett PJ (1994) The apical complex of the gregarine *Digyalum oweni* (Protozoa, Apicomplexa). J Nat Hist **28**:1–7

Edgar RC (2004) MUSCLE: multiple sequence alignment with high accuracy and high throughput. Nucleic Acids Res **32**:1792–1797

Grassé PP (1953) Classe des grégarinomorphes (Gregarinomorpha, N. nov., Gregarinae Haeckel, 1866; gregarinidea Lankester, 1885; grégarines des auteurs). In Grassé P-P (ed) Traité de Zoologie. Masson, Paris, pp 590–690

Heintzelman MB (2004) Actin and myosin in *Gregarina polymorpha*. Cell Motil Cytoskeleton **58**:83–95

Hildebrand HF (1980) Elektronenmikroskopische Untersuchungen an den Entwicklungsstadien des Trophozoiten von *Didymophyes gigantea* (Sporozoa, Gregarinida). III. Die Feinstruktur des Epizyten mit besonderer Berücksichtigung der kontraktilen Elemente. Z Parasitenkd **64**:29–46

Hopkins J, Fowler R, Krishna S, Wilson I, Mitchell G, Bannister L (1999) The plastid in *Plasmodium falciparum* asexual blood stage: a three-dimensional ultrastructural analysis. Protist **150**:283–295

Huelsenbeck JP, Ronquist F (2001) MrBayes: Bayesian inference of phylogenetic trees. Bioinformatics **17**:754–755

Köhler S (2005) Multi-membrane-bound structures of Apicomplexa: I. The architecture of the *Toxoplasma gondii* apicoplast. Parasitol Res **96**:258–272

Kuriyama R, Besse C, Gèze M, Omoto CK, Schrével J (2005) Dynamic organization of microtubules and microtubule-organizing centers during the sexual phase of a parasitic protozoan, *Lecudina tuzetae* (Gregarine, Apicomplexa). Cytoskeleton **62**:195–209

Kuvardina ON, Leander BS, Aleshin VV, Myl'nikov AP, Keeling PJ, Simdyanov TG (2002) The phylogeny of colpodellids (Alveolata) using small subunit rRNA gene sequences suggests they are the free-living sister group to apicomplexans. J Eukaryot Microbiol **49**:498–504

Landers SC, Leander BS (2005) Comparative surface morphology of marine coelomic gregarines (Apicomplexa, Urosporidae): *Pterospora floridiensis* and *Pterospora schizosoma*. J Eukaryot Microbiol **52**:23–30

Leander BS (2006) Ultrastructure of the archigregarine *Selenidium vixax* (Apicomplexa) - A dynamic parasite of sipunculid worms (host: *Phascolosoma agassizii*). Mar Biol Res **2**:178–190

Leander BS (2007) Molecular phylogeny and ultrastructure of *Selenidium serpulae* (Apicomplexa, Archigregarinia) from the calcareous tubeworm *Serpula vermicularis* (Annelida, Polychaeta, Sabellida). Zool Scripta **36**:213–227

Leander BS (2008) Marine gregarines – evolutionary prelude to the apicomplexan radiation? Trends Parasitol **24**:60–67

Leander BS, Keeling PJ (2003) Morphostasis in alveolate evolution. Trends Ecol Evol **18**:395–402

Leander BS, Ramey PA (2006) Cellular identity of a novel small subunit rDNA sequence clade of apicomplexans: Description of the marine parasite *Rhytidocystis polygordiae* n. sp. (Host: *Polygordius* sp., Polychaeta). J Eukaryot Microbiol **53**: 280–291

Leander BS, Harper JT, Keeling PJ (2003) Molecular phylogeny and surface morphology of marine aseptate gregarines (Apicomplexa): *Selenidium* spp. And *Lecudina* spp. J Parasitol **89**:1191–1205

Leander BS, Lloyd SAJ, Marshall W, Landers SC (2006) Phlogeny of marine gregarines (Apicomplexa) - *Pterospora, Lithocystis*, and *Lankesteria* - and the origin(s) of coelomic parasitism. Protist **157**:45–60

Levine ND (1971) Taxonomy of Archigregarinorida and Selenidiidae (Protozoa, Apicomplexa). J Protozool **18**:704–717

Levine ND (1976) Revision and checklist of the species of the aseptate gregarine genus *Lecudina*. Trans Am Microsc Soc **95**:695–702

Levine ND (1977a) Revision and checklist of the species (other than *Lecudina*) of the aseptate gregarine family Lecudinidae. J Protozool **24**:41–52

Levine ND (1977b) Checklist of the species of the aseptate gregarine family Urosporidae. Int J Parasitol **7**:101–108

MacMillan WG (1973) Conformation changes in the subpellicular region during peristaltic movements of a gregarine trophozoite. J Protozool **20**:267–274

Maddison DR, Maddison WP (2005) MacClade 4.08. Sinauer Associates, Inc. Sunderland

Mellor JS, Stebbings H (1980) Microtubules and the propagation of bending waves by the archigregarine, *Selenidium fallax*. J Exp Biol **87**:149–161

Ormières R, Daumal J (1970) Ultrastructural data on *Epicavus araeoceri* Orm. Daum., eugregarina parasite of *Araecocerus fasciculatus* de Geer (coleoptera Anthribidae). C R Acad Sci Hebd Seances Acad Sci D **20**:2451–2453

Perkins FO, Barta JR, Clopton RE, Pierce MA, Upton SJ (2002) Phylum Apicomplexa. In Lee JJ, Leedale GF, Bradbury P (eds) The Illustrated Guide to the Protozoza. 2nd edn Allen Press Inc., Lawrence, Kansas, pp 190–304

Porter A (1908) Merogregarina amaroucii, n g. , n. sp., a sporozoon from the digestive tract of the ascidian, *Amaroucium* sp. Arch Protistenkd **15**:227–248

Posada D, Crandall KA (1998) MODELTEST: testing the model of DNA substitution. Bioinformatics **14**:817–818

Ray HN (1930) Studies on some protozoa in polychaete worms. I. Gregarines of the genus *Selenidium*. Parasitology **22**:370–400

Ronquist F, Huelsenbeck JP (2003) MRBAYES 3: Bayesian phylogenetic inference under mixed models. Bioinformatics **19**:1572–1574

Rueckert S, Leander BS (2009) Molecular phylogeny and surface morphology of marine archigregarines (Apicomplexa), *Selenidium* spp. , *Filipodium phascolosomae* n. sp., and *Platyproteum* n. gen. and comb. from north-eastern pacific peanut worms (Sipuncula). J Eukaryot Microbiol **56**: 428–439

Rueckert S, Chantangsi C, Leander BS (2010) Molecular systematics of marine gregarines (Apicomplexa) from Northeastern Pacific polychaetes and nemerteans, with descriptions of three new species: *Lecudina phyllochaetopteri* sp. nov., *Difficilina tubulani* sp. nov., and *Difficilina paranemertis* sp. nov. Int J Syst Evol Microbiol **60**:2681–2690

Rueckert S, Villette P, Leander BS (2011a) Species boundaries in gregarine apicomplexans: A case study comparison of morphometric and molecular variability in *Lecudina* cf. *tuzetae* (Eugregarina, Lecudinidae). J Eukaryot Microbiol **58**: 275–283

Rueckert S, Wakeman KC, Leander BS (2013) Discovery of a diverse clade of gregarine apicomplexans from Pacifc eunicid polychaetes, including descriptions of *Paralecudina* gen. n., *Trichotokara japonica* n. sp., and *T. eunicae* n. sp. J Eukaryot Microbiol **60**:121–136

Schrével J (1968) L'ultrastructure de la région antérieure de la grégarine *Selenidium* et son intérêt pour l'étude de la nutrition chez les sporozoaires. J Microsc Paris **7**:391–410

Schrével J (1971a) Observations biologique et ultrastructurales sur les Selenidiidae et leurs conséquences sur la systématique des grégarinomorphes. J Protozool **18**: 448–470

Schrével J (1971b) Contribution a l'étude des Selenidiidae parasites d'annélides polychètes. II. Ultrastructure de quelques trophozoïtes. Protistologica **7**:101–130

Simdyanov TG, Kuvardina ON (2007) Fine structure and putative feeding mechanism of the archigregarine *Selenidium orientale* (Apicomplexa: Gregarinomorpha). Eur J Protistol **43**:17–25

Stebbings H, Boe GS, Garlick PR (1974) Microtubules and movement in the archigregarine, *Selenidium fallax*. Cell Tissue Res **148**:331–345

Swofford DL (1999) Phylogenetic Analysis Using Parsimony (and other Methods) PAUP* 4.0. Sinauer Associates, Inc, Sunderland, MA

Théodoridès J (1984) The phylogeny of the Gregarinia. Origins of Life **13**:339–342

Tomova C, Geerts WJ, Muller-Reichert T, Entzeroth R, Humbel BM (2006) New comprehension of the apicoplast of *Sarcocystis* by transmission electron tomography. Biol Cell **98**:535–545

Valigurová A (2012) Sophisticated adaptations of *Gregarina cuneata* (Apicomplexa) feeding stages for epicellular parasitism. PLoS ONE **7(8)**:e42606

Valigurová A, Vaškovicová N, Musilová N, Schrével J (2013) The enigma of eugregarine epicytic folds: where gliding motility originates? Front Zool **10**:57

Vivier E, Schrével J (1964) Étude au microscope électronique de une grégarine du genre *Selenidium*, parasite de *Sabellaria alveolata*. J Microsc Paris **3**:651–670

Wakeman KC, Leander BS (2012) Molecular phylogeny of pacific archigregarines (Apicomplexa), including descriptions of *Veloxidium leptosynaptae* n. gen., n. sp., from the sea cucumber *Leptosynapta clarki* (Echinodermata), and two new species of *Selenidium*. J Eukaryot Microbiol **59**: 232–245

Wakeman KC, Leander BS (2013a) Identity of environmental DNA sequences using descriptions of four novel gregarine parasites, *Polyplicarium* n. gen. (Apicomplexa), from capitellid polychaetes. Mar Biodiv **43**:133–147

Wakeman KC, Leander BS (2013b) Molecular phylogeny of marine gregarine parasites (Apicomplexa) from tube-forming polychaetes (Sabellariidae, Cirratulidae and Serpulidae), including descriptions of two new species of *Selenidium*. J Eukaryot Microbiol **60**:514–525

Zwickl D (2006) Genetic Algorithm Approaches for the Phylogenetic Analysis of large Biological Sequence Datasets under the Maximum Likelihood Criterion. PhD thesis, University of Texas at Austin